Marine Physical Laboratory

Observations of Breaking Waves Using Vertical Line Arrays

Li Ding

Supported by the
Chief of Naval Research
Grant N00014-90-J-1275

MPL Technical Memorandum 448

MPL-U-108/95
November 1995

Approved for public release; distribution is unlimited.

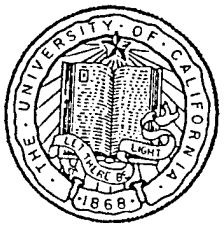

University of California, San Diego
Scripps Institution of Oceanography

REPORT DOCUMENTATION PAGE

Form Approved OMB No. 0704-0188

1. Agency Use Only (Leave Blank).

2. Report Date. November 1995

3. Report Type and Dates Covered. Technical Memorandum

4. Title and Subtitle.

Observations of Breaking Waves Using Vertical Line Arrays

5. Funding Numbers.

N00014-90-J-1275

Project No.
Task No.

6. Author(s).

Li Ding

7. Performing Monitoring Agency Names(s) and Address(es).

University of California, San Diego
Marine Physical Laboratory
Scripps Institution of Oceanography
San Diego, California 92152

8. Performing Organization Report Number.

MPL-U-108/95
MPL TM-448

9. Sponsoring/Monitoring Agency Name(s) and Address(es).

Chief of Naval Research
Department of the Navy
800 North Quincy Street
Arlington, VA 22217-5660

10. Sponsoring/Monitoring Agency Report Number.

11. Supplementary Notes.

12a. Distribution/Availability Statement.

Approved for public release; distribution is unlimited.

12b. Distribution Code.

13. Abstract (Maximum 200 words).

Ambient noise data were collected with two vertical arrays during a surface breaking wave experiment conducted 22 March-5 April 1995, North East of San Clemente Island. Conventional beamforming is applied to the data and the beamformed outputs reveal signatures of acoustic sources moving across the sea surface. Simultaneous video observations confirm that the detected acoustic sources are indeed associated with breaking surface waves. Further efforts are needed to develop an event identifications scheme for systematic analysis of the data.

14. Subject Terms.

ambient noise, vertical line arrays, surface breaking waves, wavenumber-frequency analysis, source localization

15. Number of Pages. 29

16. Price Code.

17. Security Classification of Report.	18. Security Classification of This Page.	19. Security Classification of Abstract..	20. Limitation of Abstract.
Unclassified	Unclassified	Unclassified	None

Observations of Breaking Waves Using Vertical Line Arrays

Li Ding

Marine Physical Laboratory, Scripps Institution of Oceanography, University of California, San Diego, La Jolla, CA 92093-0238.

Abstract

Ambient noise data were collected with two vertical arrays during a surface breaking waves experiment conducted 22 March–5 April 1995, North East of San Clemente Island. Conventional beamforming is applied to the data and the beamformed outputs reveal signatures of acoustic sources moving across the sea surface. Simultaneous video observations confirm that the detected acoustic sources are indeed associated with breaking surface waves. Further efforts are needed to develop an event identification scheme for systematic analysis of the data.

1 Introduction

It has long been known that wave breaking at the ocean surface generates sound which is recognized as the main source of wind-generated ambient noise. Recently, this sound has been used by Ding and Farmer (1992, 1994) to track individual breaking waves and measure their statistical properties, with a broadband (5.5 kHz) four-hydrophone array. However, because of the simplicity of the array they used and strong background noise at high winds, the array had to be deployed close to the surface (25 m below). This limited the observation area to a radius of 30-40 m, and also suffered from loss of coherence of signals when the dimension of breaking waves is large as viewed from the array (Farmer and Ding, 1992). In order to increase the observation area and reduce the finite source dimension effect, one must use a larger array and deploy it at a greater depth.

Several large-dynamic range acoustic arrays were developed at the MPL of Scripps Institution of Oceanography, for an ONR reverberation program. One potential configuration of these arrays was as a tripod array for measuring surface reverberation (Baggeroer and Hodgkiss, 1990). Each leg of the tripod would have 64 elements with 1.875 m spacing and 750 Hz bandwidth. The depth of the apex and the angle of the legs relative to the vertical would be adjusted as required. The arrays were taken on a recent field experiment for a feasibility study of using such a tripod configuration to observe breaking surface waves. Due to some deployment

difficulties, however, only two legs were deployed as vertical line arrays. In this report, we present the data collected with the two vertical arrays.

2 Experiment

The surface breaking waves experiment was conducted 22 March– 5 April. 1995. near San Clemente Island. The water depth was 200 m. For most of the period. the sea was rather calm, and there were essentially no visible breaking waves. However, on the last two days, winds started to pick up, and the wind speed reached 20 knots. At the beginning of the experiment, one of FLIP's mooring lines was broken, and the tripod array could not be deployed as planned. Instead, two legs were deployed vertically. They were approximately 31 m apart horizontally, and the top hydrophones were 10 m below the surface. The length of the arrays is 120 m, so the deepest hydrophones were about 70 m above the sea floor. A video camera was also installed to monitor the overhead area of one of the arrays (denoted as A1). A Doppler sonar system was mounted on FLIP to measure wave spectra.

3 Data Analysis

Delay-and-Sum Beamforming

Data analysis has been focused on a 10 min data set at high wind speeds (starting time: 92:031949; wind speed= 10 m/s). The data from each hydrophone were first high-passed at 200 Hz to remove low frequency interferences (to be discussed later), and then beamforming was performed on each array. Spherical waves are assumed in the beamforming. Specifically, let $\mathbf{r}_s$ be the focus location and $\mathbf{r}_i$ the location of each hydrophone. Then the data at the ith hydrophone are delayed by $\tau_i = |\mathbf{r}_s - \mathbf{r}_i|/C$, where C is the sound speed in water and is assumed to be 1500 m/s throughout the calculation below. Let $f_i(t)$ denote the acoustic signal from the ith hydrophone. Then the delay-and-sum output

$$f(t) = \sum_i f_i(t + \tau_i)$$

is squared and averaged over time to obtain power

$$P(\mathbf{r}_s) = \frac{1}{T}\int_0^T f^2(t)dt.$$

By changing $\mathbf{r}_s$, we obtain the array response to various focus locations. Since we are interested in discerning surface noise sources, $\mathbf{r}_s$ is constrained on the surface and chosen to start from the overhead of the array and increase in the radial direction. The averaging time was chosen to be T=512/1500=0.34 s. For each T, we scan from $r_s = 0$ to $r_s = 100$ m, and repeat the scanning continuously throughout the entire data set (the shell script program is given in Appendix B).

Source Localization

Let d be the horizontal spacing of the two arrays. Let r_1 and r_2 be the horizontal range of the source location with respect to Array 1 and Array 2. If a coordinate is chosen such that A1 and A2 are located at (-d/2, 0) and (d/2, 0) respectively, then in this coordinate, the source location is found to be

$$x = \frac{1}{2d}(r_1^2 - r_2^2), \tag{1}$$

$$y^2 = \frac{1}{(2d)^2}[r_1^2 - (r_2 - d)^2][(r_2 + d)^2 - r_1^2]. \tag{2}$$

This requires that the right-handed side of Eq. (2) be positive. If not, it implies that r_1 and r_2 are not related to the same source, or that there are significant errors in measuring r_1 and r_2. It is also seen that two vertical arrays cannot uniquely determine the source location, since y can be positive or negative.

Wavenumber-Frequency Analysis

A wavenumber-frequency analysis allows separation of signals with different propagation speeds, even if they have close frequency components and angles of arrival. Let $f(z_i, t_l)$ be the signal output at each individual hydrophone. Its 2D FFT

$$F(k_z, \omega) = \sum_i \sum_l f(z_i, t_l) \exp\{-j\omega t_j - jk_z z_l\} \tag{3}$$

decomposes the signal into various temporal and spatial frequency components. Note that in the case of a vertical array, k_z and ω are related by

$$k_z = \frac{\omega}{C_p} \cos\theta, \tag{4}$$

where θ is the angle relative to the vertical and C_p the propagation speed. Signals with different C_p will be manifested as linear patterns with different slopes in the $k_z - \omega$ plot (i.e. an image plot of $F(k_z, \omega)$). The purpose of such an analysis is to identify interference due to vibration of cables that connect the hydrophones. In practical implementations, data are broken into a number of segments in time and FFTs are performed on each segment. Then a single FFT of size 64 is performed on space, and the results are squared and averaged over segments (see the script program in Appendix C).

4 Results and Discussions

Figure 1 shows a short period of (60 s) of the beamformed output from $A1$ (the starting time is also shown). The horizontal axis is the horizontal range r relative to the array, and the vertical axis is time. There are some dark bands across the entire range, which are believed to be due to vibrations of the cables which the hydrophones

were tied to. Such vibrations were caused primarily by wave motions, especially when there were large breaking waves nearby. A wavenumber-frequency analysis of the data covering the dark bands shows a strong low frequency-wavenumber component, despite a 50 dB rejection in the stopband of the high-pass filter. For example, Fig. 2 shows the wavenumber-frequency spectrum of the data covering the second band (12th-14th second) in Fig. 1, where there are signals with frequency below 50 Hz and wavenumber less than 0.33 rad/m. The 50 Hz component also extends across the entire k-space (see Fig. 9b where no highpass filtering was performed). This feature does not exist when the data are outside the bands. There are also dark patches in Fig. 1 located constantly at range 30 m throughout the time. These are believed to result from FLIP's engine noise coupled into the water and will be seen more clearly in Fig. 3.

The beamformed output is also normalized by the maximum in each scan as shown in Fig. 3. This helps suppress some of the more distinguished bands, but additional bands (usually narrower) are also introduced or enhanced. We also see some inclined streaks in Figs. 1 and 3. These indicate moving sources which are believed to be associated with breaking events as explained below. The normalization (Fig. 3) appears to enhance the streaks relative to their neighborhood. Other enhancement techniques were also tried and they are discussed and presented in Appendix A. However, we only visually analyse events based on the normalization, and future work is required to develop an automatic event selection scheme based on enhanced images.

We now associate the streaks in Fig. 3 with breaking events and mark them by event number. The video indicates that Event 2 in Fig. 3 (16th-20th second) coincided with a large whitecap moving across the overhead of $A1$, and three snapshots of the video during the occurrence of Event 2 are given in Figs. 4a-4c. The whitecap was moving into the screen from the left. Fig. 4a shows the early stage in which the whitecap was relatively compact. Then the wave crest moved towards the array leaving foams behind (Fig. 4b), and finally the wave passed the array and decayed (Fig. 4c). The pattern associated with Event 2 in Fig. 3 appears consistent with Fig. 4.

Figure 5 shows the array output of $A2$ with the same normalization. Event 1, although shown clearly in Fig. 3 moving from r_1=50 m to r_1=30 m, is smeared in Fig. 5, showing no clear moving trend. This may be due in part to the finite size effect encountered in the earlier work by Ding and Farmer (1992). The second half part of Event 2 in Fig. 3 (leaving $A1$) does not appear in Fig. 5 and this part cannot be tracked. There are also events that were identified in the video and the beamformed output of $A1$, but not in the output of $A2$. Visual inspection on the video indicates that these events occurred at such locations that FLIP's body was between them and $A2$; thus the acoustic signals arriving at $A2$ may have been obscured by the presence of FLIP, which would be another factor that prevents us from seeing the same event clearly on both arrays. The smearing of Event 1 may also result from the presence of FLIP, since as seen in Fig. 6 below, FLIP was between Event 8 and $A2$ (Event 1 in Fig. 3 is marked as Event 8 in Fig. 6).

From this 10 min data set, we were able to collect visually 10 events that appear

clearly on both arrays. For simplicity, we draw a line on each streak, thus obtaining a linear $r - t$ relation. We then use Eqs.(1) and (2) to determine and track their locations. Fig. 6 shows the trajectories of these events, where $A1$, $A2$ and F indicate the locations of Array 1 and Array 2, and FLIP. Events 3 and 7 show no moving trends, so we only plot their locations as circles. It has been mentioned earlier that there are two solutions for the same source location, and the broken lines in Fig. 6 indicate the second solution. These two solutions are separated by the line connecting $A1$ and $A2$. The wind during the time was blowing from the lower-left corner to the upper-right corner, so it appears that the solid lines represent the true trajectories except for Events 2, 6, 10.

Among these events, Events 1, 3, 4, 5, 7, 9 were also observed on the video based on their times of occurrence. The whitecap in Fig. 4 corresponds to Event 9 in Fig. 6. Fig. 7 is a sketch of the whitecaps as seen on a TV screen. The numbers correspond to those in Fig. 6. The true distance from each event to the array needs calibration before doing any serious comparison. However, the trajectories or locations shown here in Fig. 6 appear consistent with what were observed on the video (Fig. 7). We therefore conclude that these dark streaks in the acoustic images are due to visible whitecaps, or breaking waves.

The speeds of these events except Events 3 and 7 were also determined, and are shown in Table 1. These range from 4.6 m/s to 9 m/s, with Event 8 having an exceptional speed of 16 m/s. This could be due to the uncertainty in measuring r_2 from $A2$ (Fig. 5). The remaining 7 events have a mean speed of 6.9 m/s. If the travel speed is taken to be the phase speed, this would correspond to a wave period of 4.4 s. However, these numbers do not represent significant statistics since only 7 events were included.

These data also allow us to examine the frequency components of the signal generated by an individual wave. Take Event 2 in Fig. 3 as an example. Figure 8 shows a series of power spectra of the array beamformed output (delay-and-sum output, no high-pass filtering). The focus location is $r = 15$ m, i.e. the range of Event 2 relative to $A1$. The series starts from time 15.68 s, and each power spectrum was obtained by averaging over 0.68 s. These power spectra are shown as relative to the background level (including FLIP's engine noise) measured prior to the breaking. In other words, the background spectrum is subtracted from each spectrum and the result is shown in dB (note: the difference must be all positive. This was checked before taking dB values. Otherwise the result would have to be plotted on a logarithm scale). Spectrum number 1 is the initial stage of breaking and significant increase in the sound level can be seen for frequencies up to 500 Hz. There is a peak at 50 Hz, which diminishes in Spectrum 2.

The peak picks up again in Spectrum 3, 4 and 5, and becomes substantially larger and shifts to a slightly lower frequency. The times of these spectra correspond to the dark band in Fig. 1. A wavenumber-frequency analysis was thus performed on the data corresponding to Spectrum 1 and Spectrum 4, as shown in Figs. 9a and 9b respectively. Figure 9b shows a strong low frequency component around 50 Hz across the entire wavenumber space. We believe that this is not due to a source at the sea surface and it must be due to the vibration of the cables. Fig. 9a however

Event #	1	2	4	5	6	8	9	10
Speed (m/s)	9.15	8.03	4.59	4.70	5.50	16.0	8.50	8.00

Table 1: Event speeds of the observed breaking events

shows a pattern within $k < 0.33$ rads/m and a slope of $(\omega/k_z =)$ 1330 m/s. Although this value does not give an angle of arrival based on Eq. (4) for a sound speed of 1500 m/s, it may indicate a source overhead. Therefore we speculate that Event 2 may have initially radiated low-frequency components down to tens of Hz (note that FLIP's engine noise has been subtracted). Whether or not these low-frequency components persist throughout the breaking process cannot be determined due to the vibration of the cables.

5 Concluding Remarks

We have presented in this report a preliminary analysis of the vertical array data collected during the March–April surface breaking waves experiment. Conventional delay-and-sum beamforming was performed to detect and track individual surface noise sources. So far we have been able to track relatively strong sources, and the video observations confirm that the acoustic sources were indeed associated with whitecaps or breaking waves. This also supports the earlier reports by Crowther and Hansla (1993) and Hollett (1994). Power spectral analysis of a single breaking event suggests that such an event may have radiated sound down to tens of Hz.

However, our ability to track more breaking waves in this experiment has been limited by a few factors. First, the engine noise from FLIP may have prevented us from discerning weaker events. Second, the presence of FLIP may have obscured acoustic signals arriving at either of the arrays, so that an event may be detected clearly by one array but not by the other. Third, finite source dimension may be another factor, but it is difficult to assess its significance since it has an effect similar to that due to the presence of FLIP. Further improvements can be made by pointing the broadside of the array towards the sea surface, since a line array has a much better spatial resolution beam at the broadside than at the endfire as in the present case, and by increasing the cutoff frequency so as to improve the resolution and make use of broader band information from wave-generated noise sources.

We have also applied minimum variance beamforming to the data. The results do not appear superior to those obtained with conventional beamforming, and the computation is far more expensive. One difficulty with MV beamforming is that the inversion of the covariance matrix estimated from the array data requires sufficient time averaging, which is not quite suitable for analysing signals generated by wave breaking, since breaking waves are usually a transient process.

More efficient use of the data can be made by improving the images and designing an automatic scheme to extract events. The results thus obtained can be related to the wave information acquired with the Doppler sonar. We can further examine the power spectrum of the acoustic signatures generated by individual breaking waves,

in hopes of revealing any details. However, due to vibration of the cables, careful separation of acoustic signals from mechanical signals is necessary.

Acknowledgements

This work was supported by the Office of Naval Research, Code 321, under grant N00014-90-J-1275.

References

Baggeroer, A. B. and W. S. Hodgkiss, 1990: Simulations of Reverberation Measurement uisng a Tripod Array. (abstract). *J. Acoust. Soc. Am.* 88, Supll. S85.

Crowther, P. A. and A. Hansla, 1993: The Lifetimes, Velocities and Probable Origin of Sonic and Ultrasonic Noise Sources on the Sea Surface. *Natural Physical Sources of Underwater Sound*, B. Kerman, Ed., Kluwer Academic, 379-392.

Ding, L. and D. M. Farmer, 1992: A Signal Processing Scheme for Passive Acoustical Mapping of Breaking Surface Waves. *J. Atmos. Oceanic Tech.*, Vol. 9, No. 4, 484-494.

Ding, L. and D. M. Farmer, 1994: Observations of Breaking Surface Wave Statistics. *J. Phys. Oceanogr.*, Vol. 24, No. 6, 1368-1387.

Farmer, D. M., and L. Ding, 1992: Coherent Acoustical Radiation from Breaking Waves. *J. Acoust. Soc. Am.* 92(1), 397-402.

Hollett, R. D., 1994: Observations of Underwater Sound at Frequencies below 1500 Hz from Breaking Waves at Sea. *J. Acoust. Soc. Am.* 95(1), 165-170.

A Image Processing

A careful examination on Fig. 1 shows that the power level in the dark bands rises significantly across the entire range. For example, Fig. 11a shows a plot of the beamformed output of $A2$ versus time, in which there a dark band between the 18th and 21st second. Figure 10a is a snapshot at time 17.34 s and Fig. 10b is at time 19.04 s which is inside the band. In Fig. 10a, a significant peak is located at r=20 m, while in Fig. 10b, this peak diminishes because the background also rises. Since the dynamic range in the image has to include weaker signals in other areas, finer structure in the bands cannot be revealed. The normalization in Fig. 3 partially overcomes this problem, but the result is not always satisfactory. Another approach is to remove the underlying trend in each scan. For example, we can fit the data in Fig. 10 to a simple polynomial (e.g. 2nd order), and then subtract the polynomial curve from the data. Figures 10c and 10d show the results after subtraction of the fitted curves (broken lines) from Figs. 10a and 10b. We can see the level in Fig. 10d ranges from -1 to +1 dB, and that the structures at larger range are also enhanced. If an image quantization range is chosen to be from -2 dB to 4 dB, then the levels in Fig. 10d are in the mid-range of the quantization.

Figure 11c shows the result of Fig. 11a after such processing. Compared with Fig. 11b, which is the normalization of Fig. 11a, Fig. 11c appears cleaner, with the streaks more clearly revealed above the background. In particular, the event between the 36th and 39th second shows no moving trend in Fig. 11a but appears clearly moving from r=60 m to r=80 m. However, it must be pointed out that although the band in Fig. 11a is removed in Fig. 11c, the power level appears weaker in Fig. 11c for the period of the band, whereas the actual sound during that period may still have been very loud. This image enhancement is more suitable for automatic event search than the normalization approach, but not appropriate for interpreting the sound generation process.

```
####################   APPENDIX B  ########################################
#       FBF_V.SCR: performs broadband focus beamforming on a line array.
#       Input file name required. del_Vnn is a C-program residing in the
#       current directory. Output file has a suffix '.fbf' to the input file.
#
if ($#argv != 1) then
        echo 'Input file name is needed'
        exit
endif
#define parameters
set LDATA=512
set XSTART=0
set RMAX=100
set ISCAN=42
set NA=64
#start scanning
set iscan=0
while( $iscan <= $ISCAN )
set i=`expr $iscan \* $LDATA + 1`
part $i $LDATA $1 tempdat
#start beamforming towards different locations
set XS=$XSTART
   while( $XS <= $RMAX )
#generate delays for point at (XS, 0.) using a C-program
        del_Vnn $NA $XS 0.
#convert the delay file into sio format
        point 0 delay_V$NA.txt delay_V$NA
#shift element output according to the delays using linear interpolation
        shiftchfd m delay_V$NA tempdat fbf_leg1
        meanch 0 fbf_leg1 fbf_leg1
        var 0 fbf_leg1 rms_tmp
        if ( $XS == $XSTART ) then
                mv rms_tmp rms_out
        else
                mux rms_out rms_tmp rms_out
        endif
        set XS=`expr $XS + 2`
   end
if( $iscan == 0 ) then
        mv rms_out $1.fbf
else
        concat $1.fbf rms_out $1.fbf
endif
#       echo processed index=$i":   " `date`
set iscan=`expr $iscan + 1`
end
rm rms_tmp tempdat rms_out fbf_leg1
```

```
##################### APPENDIX C ########################################
#       FREQWN.SCR: performs wavenumber-frequency analysis.
#       Assumes 64 iput channels or 64 hydrophones.
#       The file can have an arbitrary length in time.
#       Time-averaging is performed. No spatial averaging.
#               /calico8/liding                          9/22/95
#########################################################################
·if ($#argv != 1) then
        echo 'Input file name is needed'
        exit
·endif
#define parameters
set NF1=128
set LD1=128
set NF2=64
set LD2=64
set M=`expr $NF1 / 2 + 1`
echo $M
echo $LD2
#perform fft on time
fftpwrfx -j $NF1 $LD1 50 1500. $1 fftwfile$LD1 sfile$NF1 $1.out
#transpose the output for next fft operation
transp -c $1.out $1.trp
#perform fft on space
fftpwrfx -c -j $NF2 $LD2 0 0.5333 $1.trp fftwfile$LD2 sfile$NF2.2 $1.fk
#transpose the output for averaging
transp -c $1.fk $1.kf
#perform incoherent segment averaging
avg -c $M 0 $1.kf $1_kf_pwr
logmag -d $1_kf_pwr $1.kf
rm $1.out $1.trp $1.fk $1_kf_pwr
```

Figure Captions

Fig. 1: Beamformed output of Array 1 versus time. The raw data were high-passed at 200 Hz before beamforming. Each scan is averaged over 0.34 s. The horizontal range is relative to the array. Gray level represents the output power in dB. The reference level is in arbitrary unit.

Fig. 2: Wavenumber-frequency spectrum of the array data covering the period of the second band in Fig. 1 (12th-14th second). The power level is in arbitrary units. The spectrum is obtained by averaging the data over a period of 2048/1500=1.365 s. No spatial averaging is done. The size of FFT is 512 in time and 64 in space.

Fig. 3: Normalization of Fig. 1. The power output in each scan is normalized by the maximum. The inclined streaks are associated with moving sources. Event 2 is also observed on the video.

Fig. 4: Video images of the whitecap coincident with Event 2 in Fig. 3 in different stages. (a) early stage; (b) energetic stage; (c) decaying stage.

Fig. 5: Normalized beamformed output of Array 2. The period is the same as Fig. 1.

Fig. 6: A plan view of the trajectories (locations) of 10 breaking events identified on both arrays, for a period of 10 min. A1, A2, and F denote the locations of Array 1, Array 2, and FLIP. The two possible trajectories for each event are marked by a solid line and a broken line. They are separated by the line connecting A1 and A2. The arrows indicate the direction of travel. The circles denote the events that are difficult to track.

Fig. 7: A sketch of the whitecaps that appear on the video and are also observed acoustically. The sketch is drawn based on what was seen on the TV screen. Array 1 was suspended from a boom on FLIP located on the lower-right side of the sketch. The number on each whitecap corresponds to that in Fig. 6, and the arrow indicates the direction in which the whitecap is moving. The size of whitecap and the distance relative to the array are not necessarily real.

Fig. 8: A series of power spectra for the data in Fig. 1, starting from time 15.68 s. The length of the data is 1024 points (0.68 s) for each spectrum. The FFT size is 128 with 50% overlap. Note that the background spectrum was subtracted.

Fig. 9: Wavenumber-frequency of the data in Spectrum 1 and Spectrum 4 of Fig. 8. The data length is 1024 and the FFT size 128 in time and 64 in space. The difference between this figure and Fig. 2 is that no highpass filtering was performed here.

Fig. 10: Snapshots of the beamformed output shown in Fig. 9a at two different instants. (a) Before the dark band in Fig. 9a; (b) in the dark band. The

broken lines are a 2nd-order polynomial fit of the data. (c) Result of trend removal of (a); (d) result of trend removal of (d).

Fig. 11: (a) An image plot of the beamformed output of Array 2; (b) normalization of (a); (c) trend removal (2nd-order polynomial) of (a).

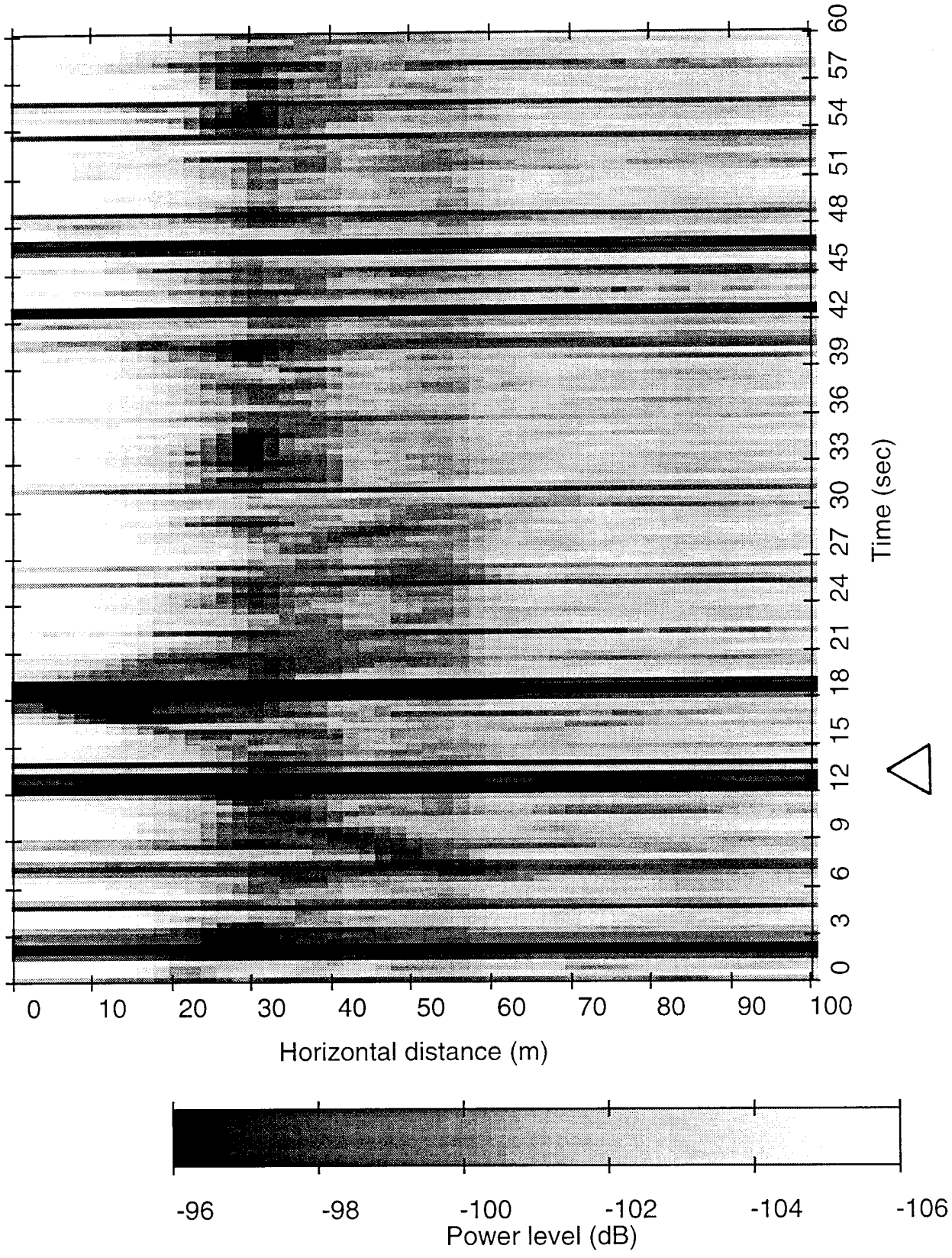
Focus beamformed output v.s. time
File: tapeV46.10.sio
Start Time: 092:032749
0 3 6 9 12 15 18 21 24 27 30 33 36 39 42 45 48 51 54 57 60
Time (sec)
0 10 20 30 40 50 60 70 80 90 100
Horizontal distance (m)
-96 -98 -100 -102 -104 -106
Power level (dB)

Figure 1.

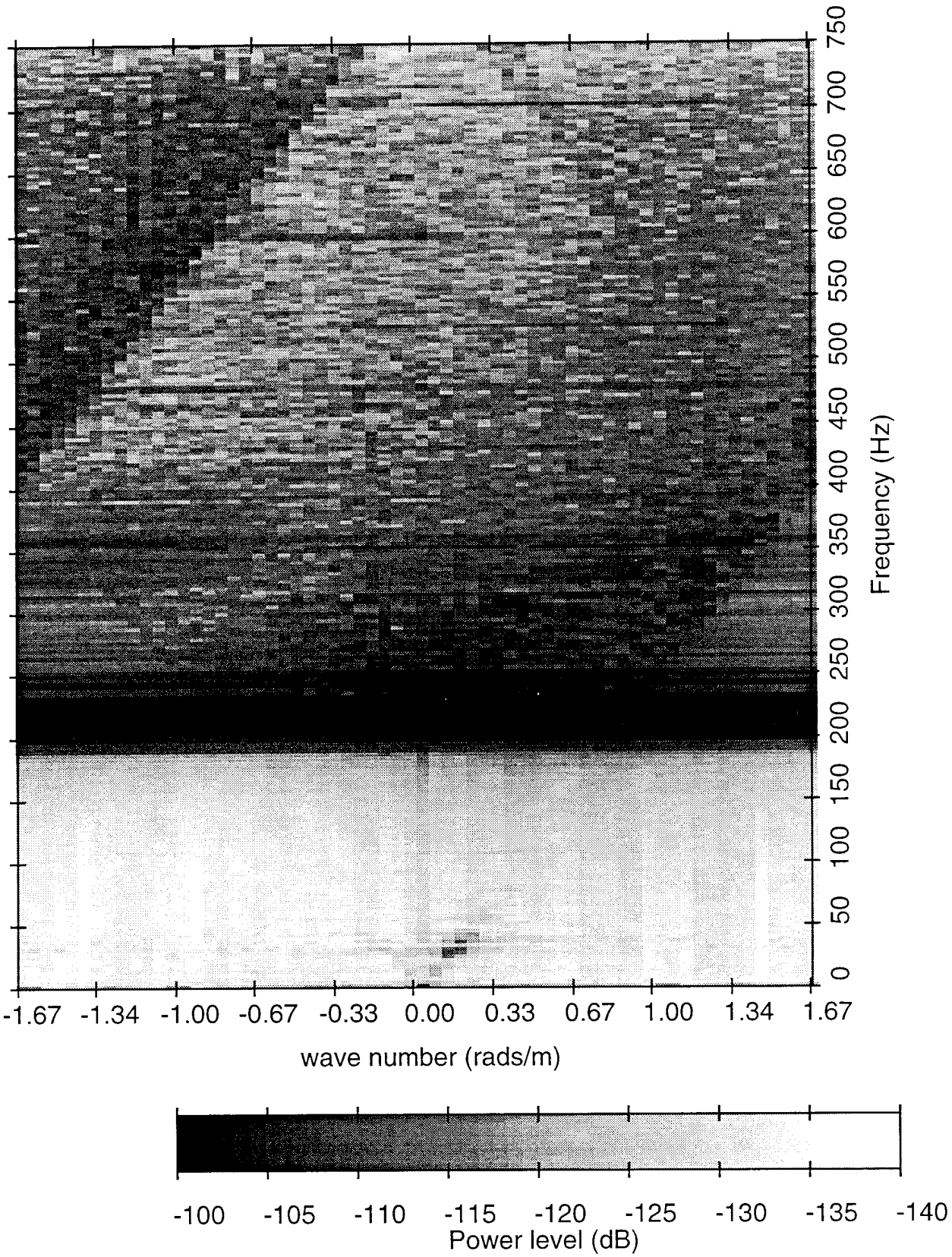
Wavenumber-Frequency Spectrum
File: tape46.10.sio, (C)
Start Time: 092:032801
750
700
650
600
550
500
450
400
350
300
250
200
150
100
50
0
Frequency (Hz)
-1.67 -1.34 -1.00 -0.67 -0.33 0.00 0.33 0.67 1.00 1.34 1.67
wave number (rads/m)
-100 -105 -110 -115 -120 -125 -130 -135 -140
Power level (dB)

Figure 2.

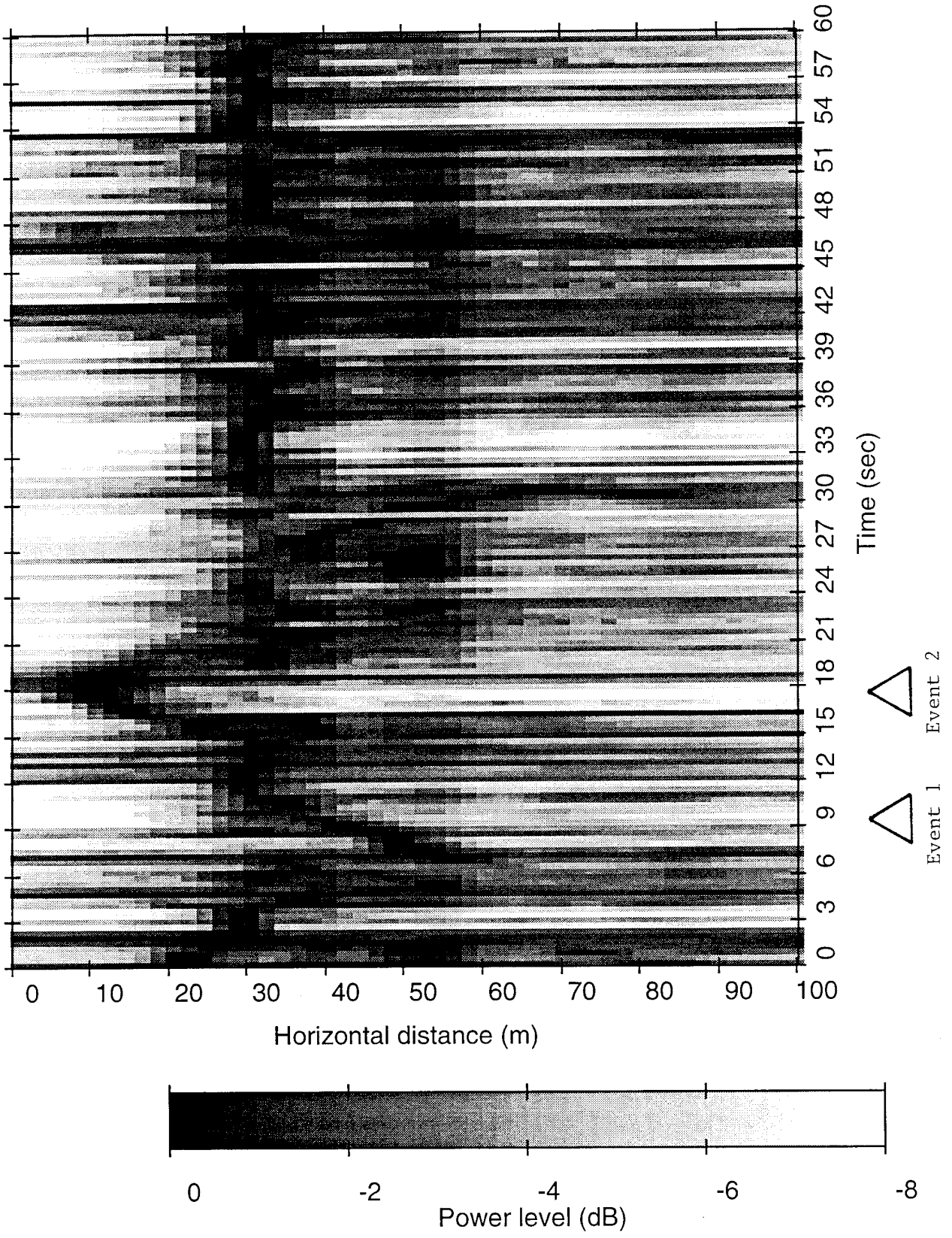
Focus beamformed output v.s. time
File: tapeV46.10.sio, normalized
Start Time: 092:032749
0 3 6 9 12 15 18 21 24 27 30 33 36 39 42 45 48 51 54 57 60
Time (sec)
Event 1
Event 2
0 10 20 30 40 50 60 70 80 90 100
Horizontal distance (m)
0 -2 -4 -6 -8
Power level (dB)

Figure 3.

Figure 4a.

Figure 4b.

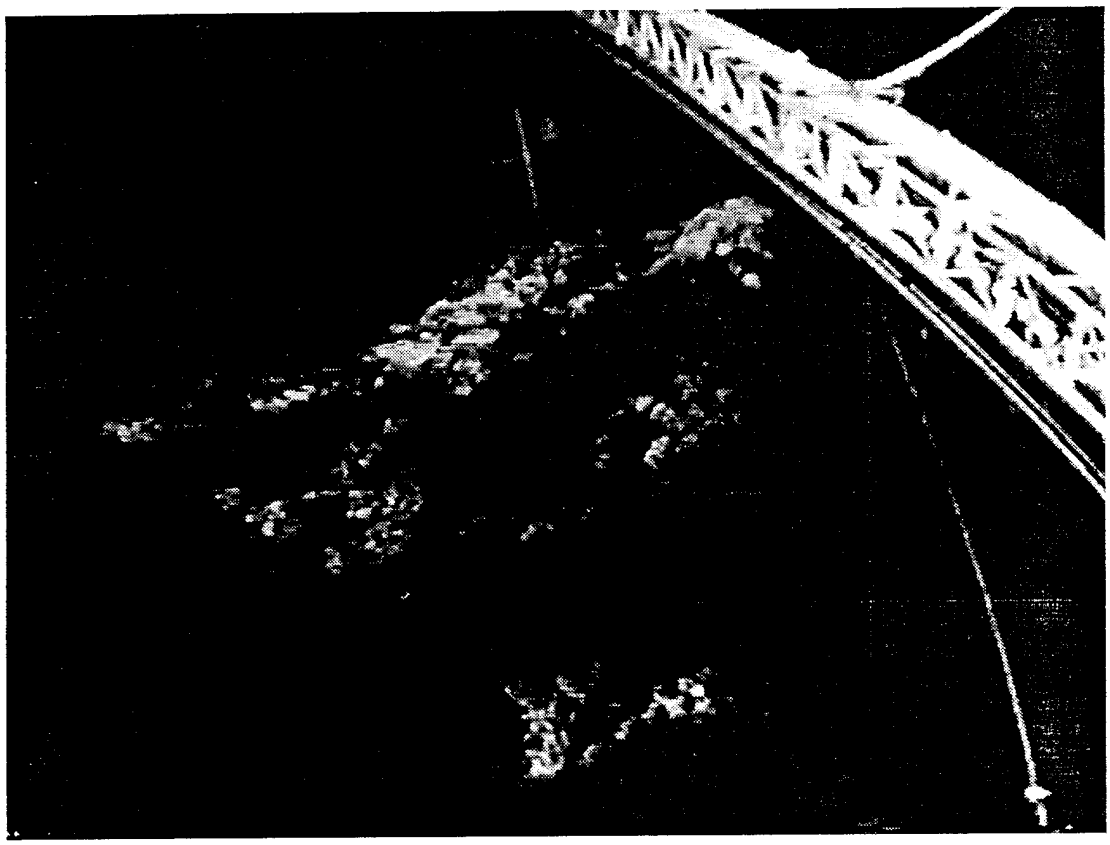

Figure 4c.

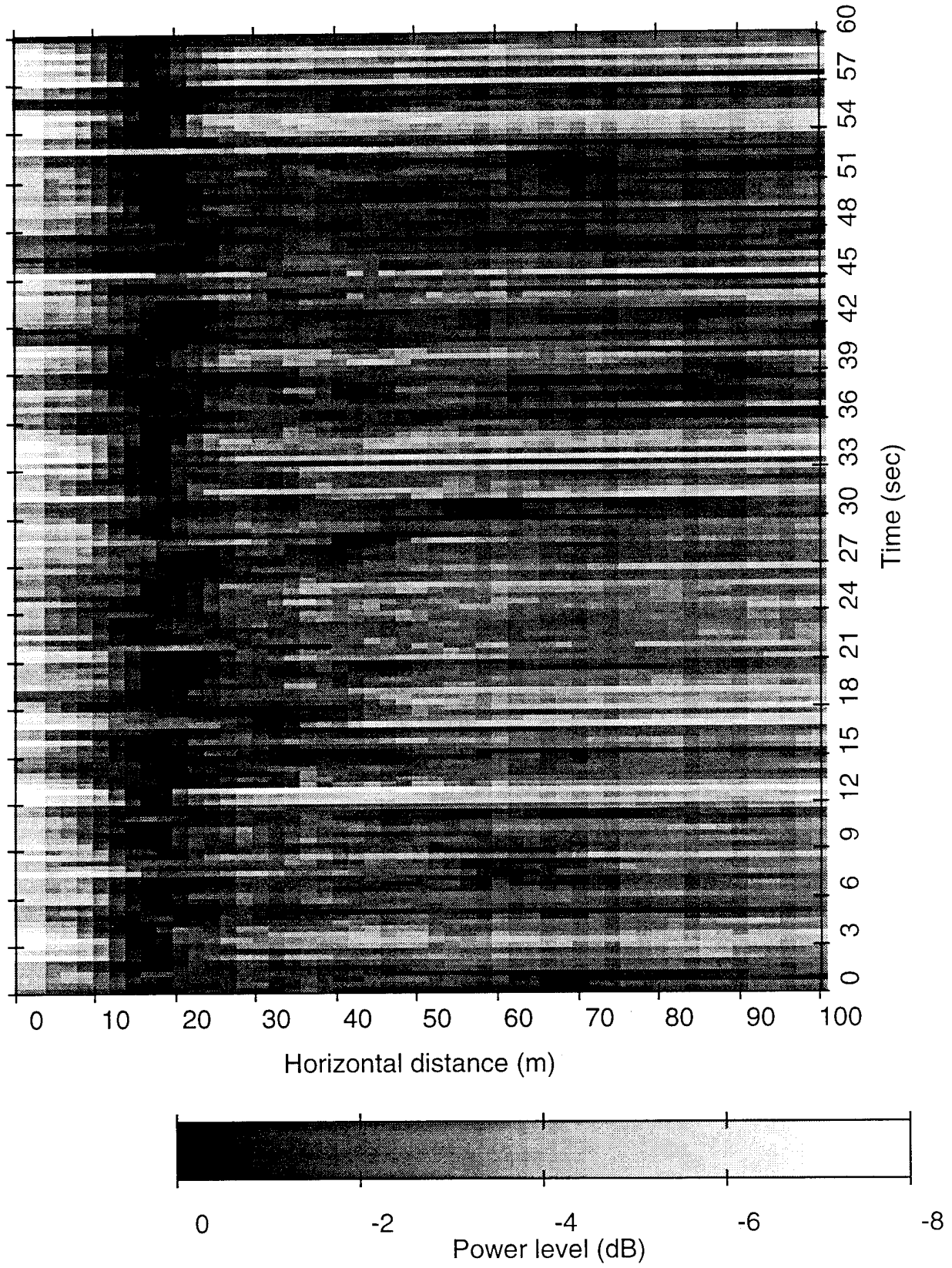
Focus beamformed output v.s. time
File: tapeE25.10.sio, normalized
Start Time: 092:032749
0 3 6 9 12 15 18 21 24 27 30 33 36 39 42 45 48 51 54 57 60
Time (sec)
0 10 20 30 40 50 60 70 80 90 100
Horizontal distance (m)
0 -2 -4 -6 -8
Power level (dB)

Figure 5.

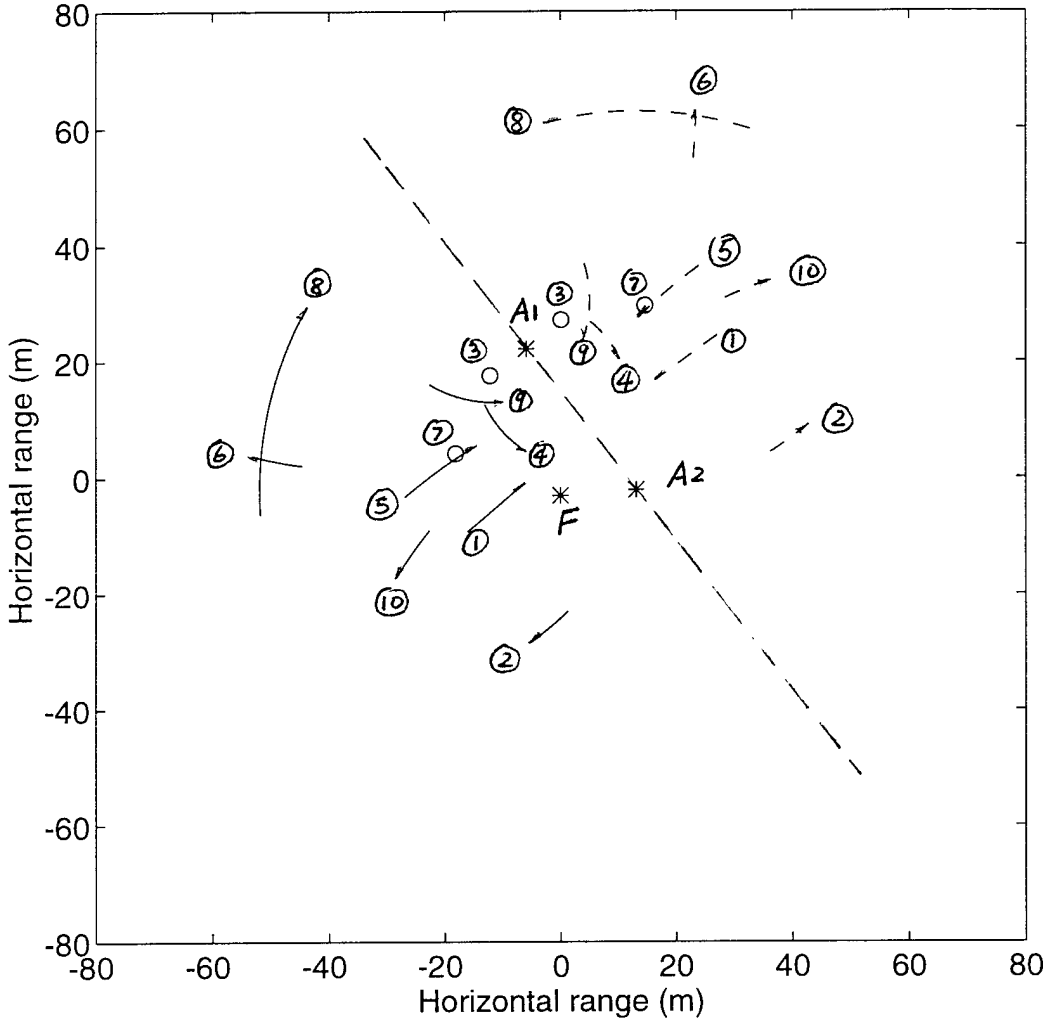
Horizontal range (m)
Horizontal range (m)
80
60
40
20
0
-20
-40
-60
-80
-80
-60
-40
-20
0
20
40
60
80
A1
A2
F

Figure 6.

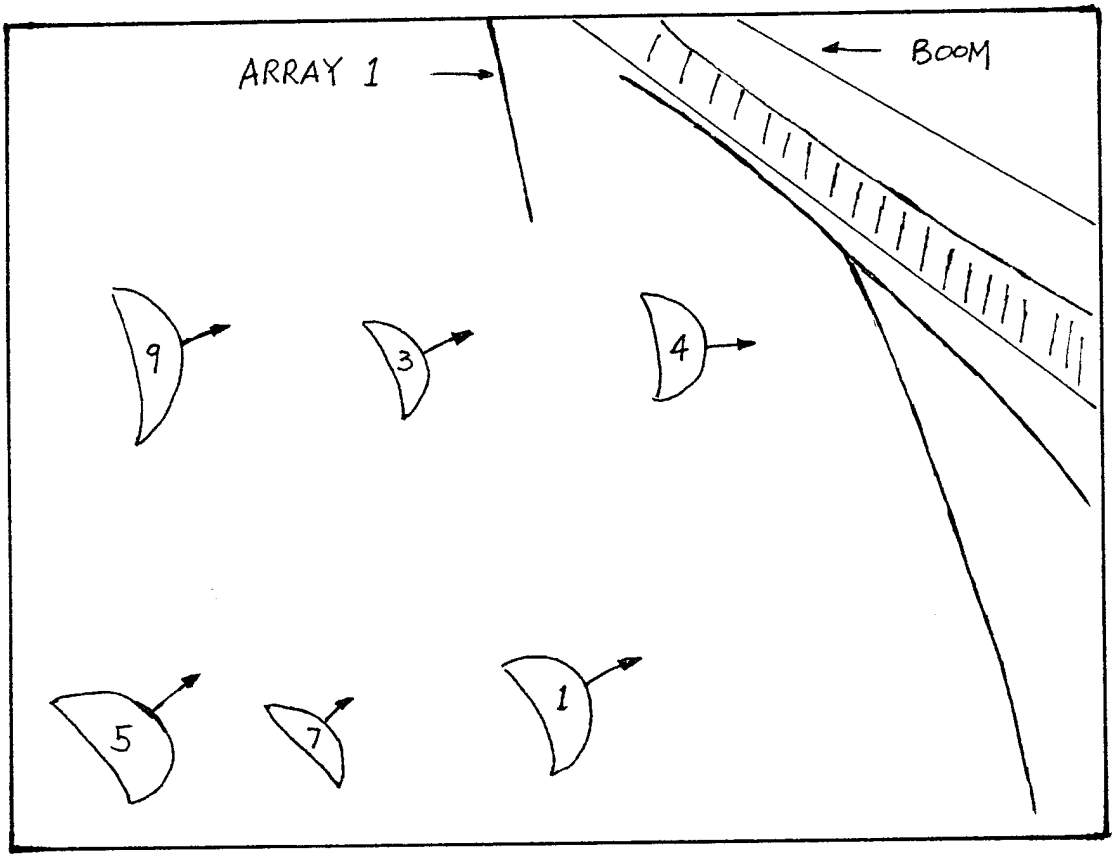

Figure 7.

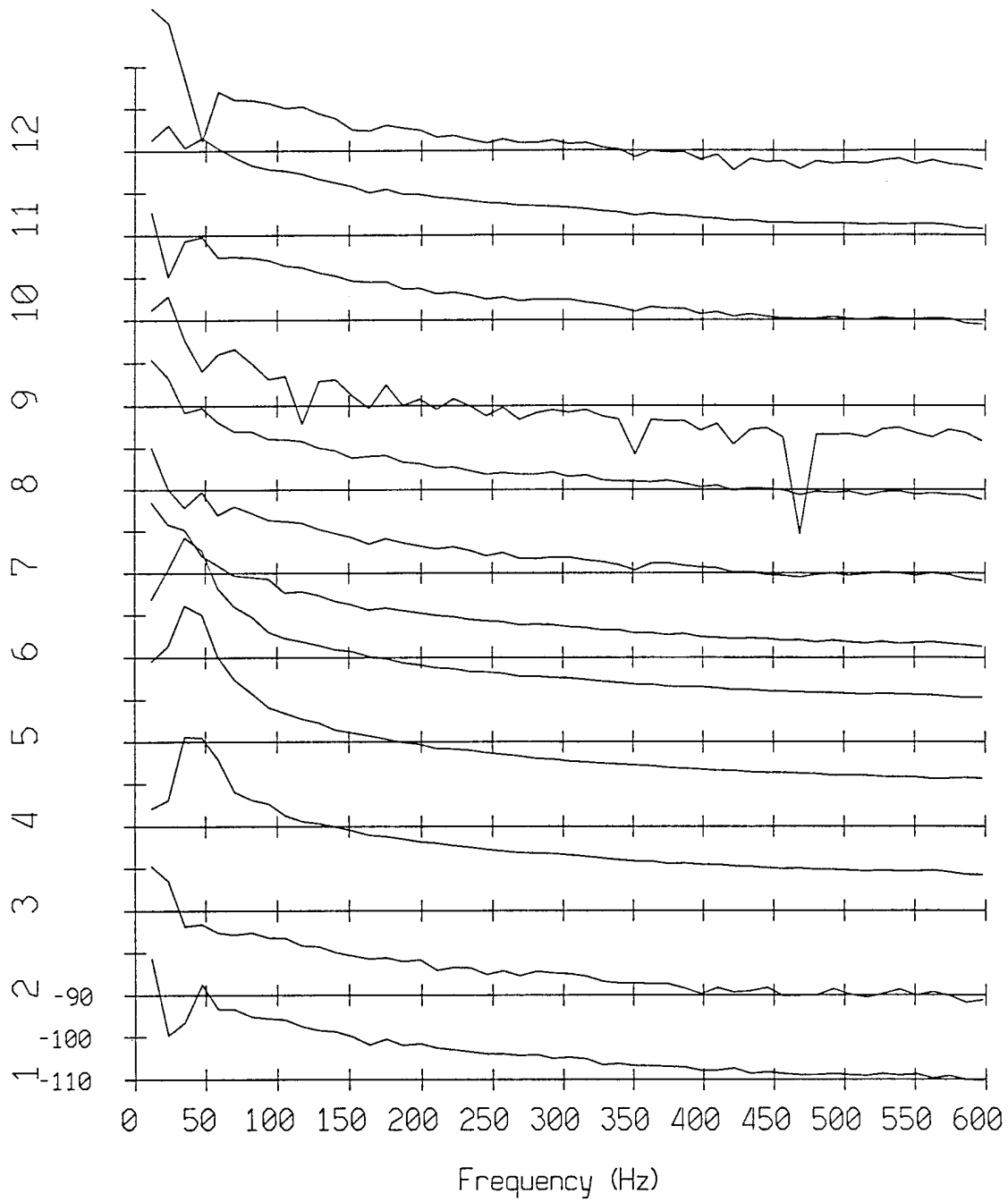
12
11
10
9
8
7
6
5
4
3
2
1
-90
-100
-110
0
50
100
150
200
250
300
350
400
450
500
550
600
Frequency (Hz)

Figure 8.

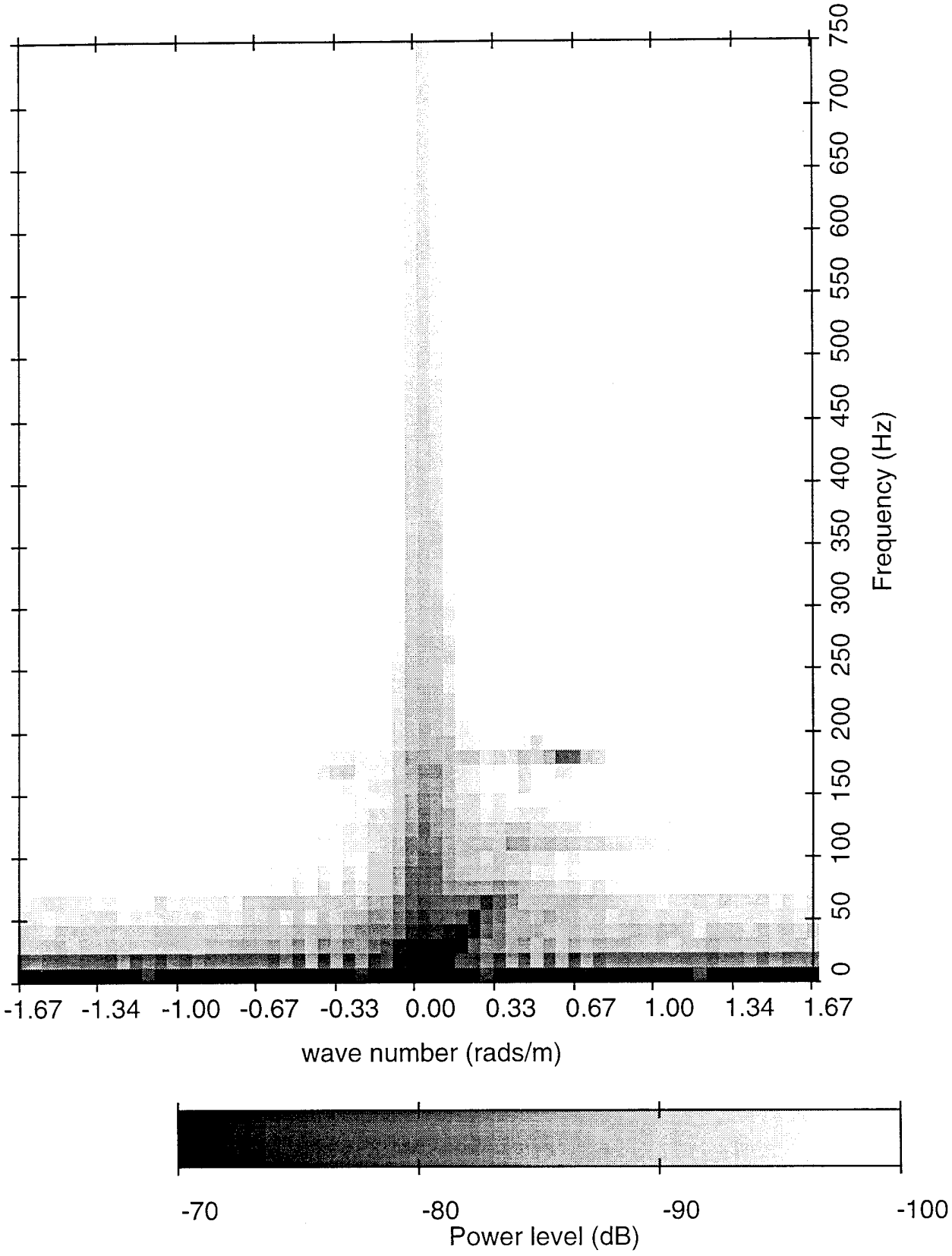
Wavenumber-Frequency Spectrum
File: tapeV46.10.sio
Start Time: 092:032804.68
750
700
650
600
550
500
450
400
350
300
250
200
150
100
50
0
Frequency (Hz)
-1.67
-1.34
-1.00
-0.67
-0.33
0.00
0.33
0.67
1.00
1.34
1.67
wave number (rads/m)
-70
-80
-90
-100
Power level (dB)

Figure 9a.

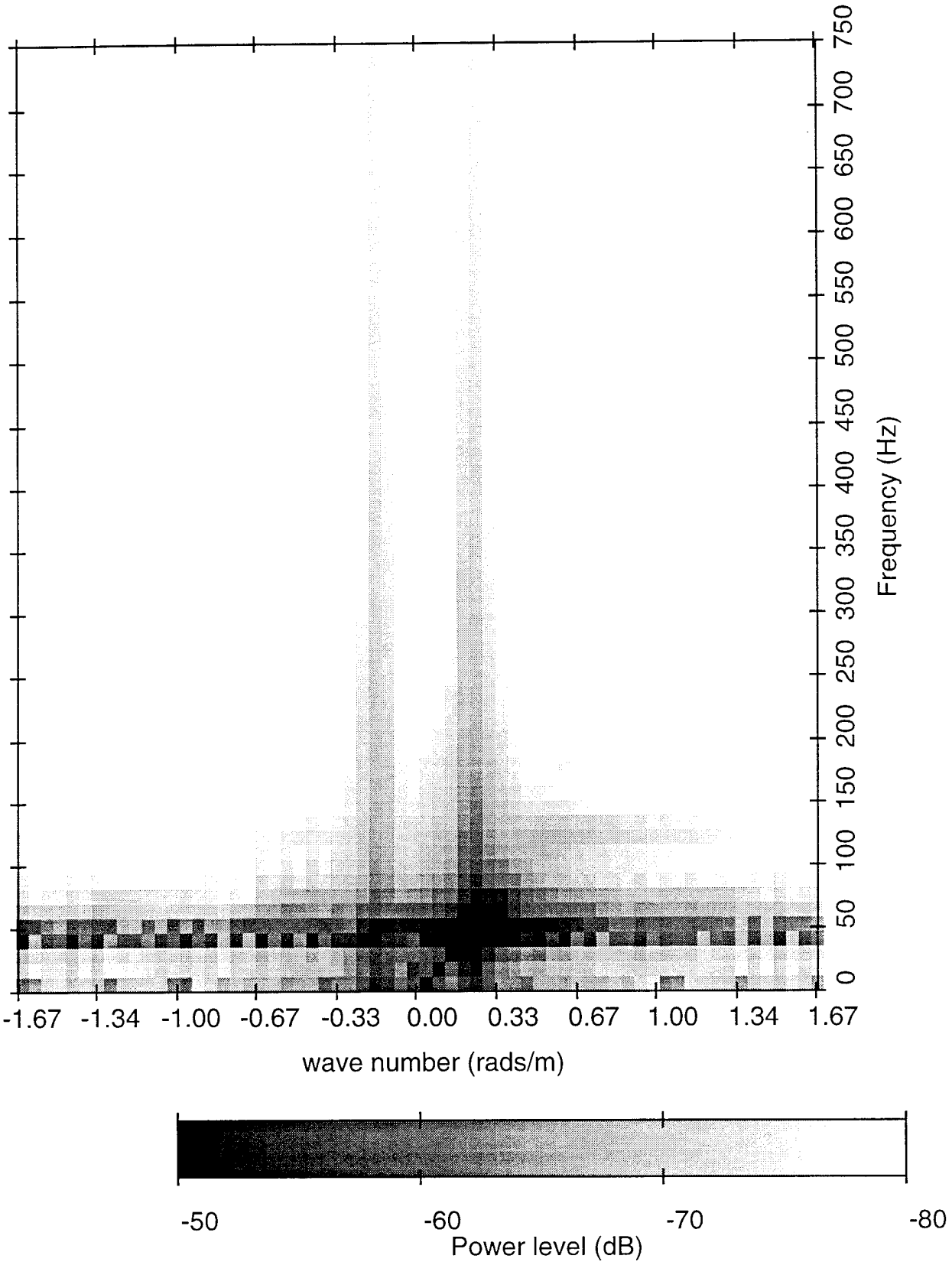
Wavenumber-Frequency Spectrum
File: tapeV46.10.sio
Start Time: 092:032806.72
750
700
650
600
550
500
450
400
350
300
250
200
150
100
50
0
Frequency (Hz)
-1.67
-1.34
-1.00
-0.67
-0.33
0.00
0.33
0.67
1.00
1.34
1.67
wave number (rads/m)
-50
-60
-70
-80
Power level (dB)

Figure 9b.

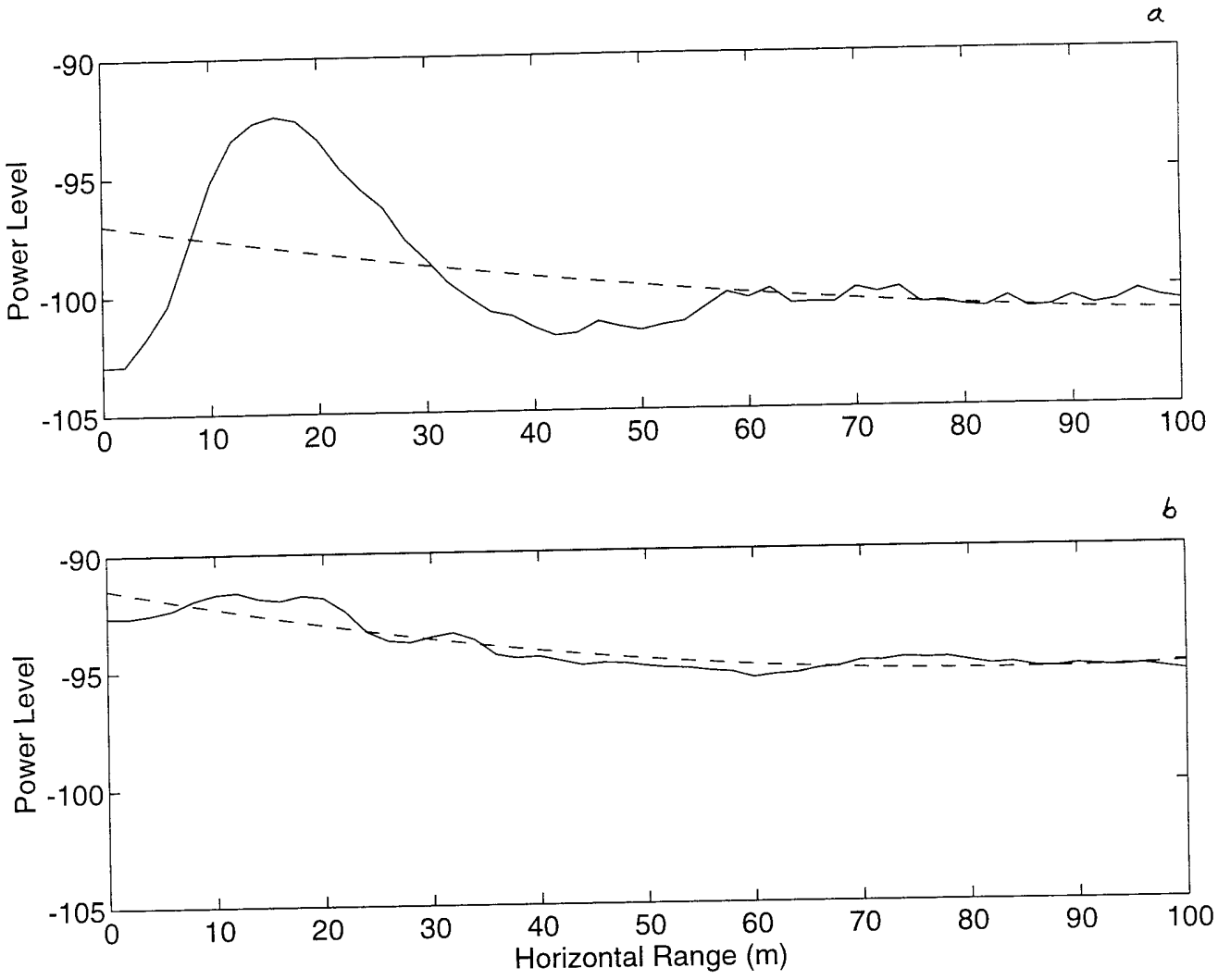
a
-90
-95
-100
-105
Power Level
0
10
20
30
40
50
60
70
80
90
100
b
-90
-95
-100
-105
Power Level
0
10
20
30
40
50
60
70
80
90
100
Horizontal Range (m)

Figure 10a,b.

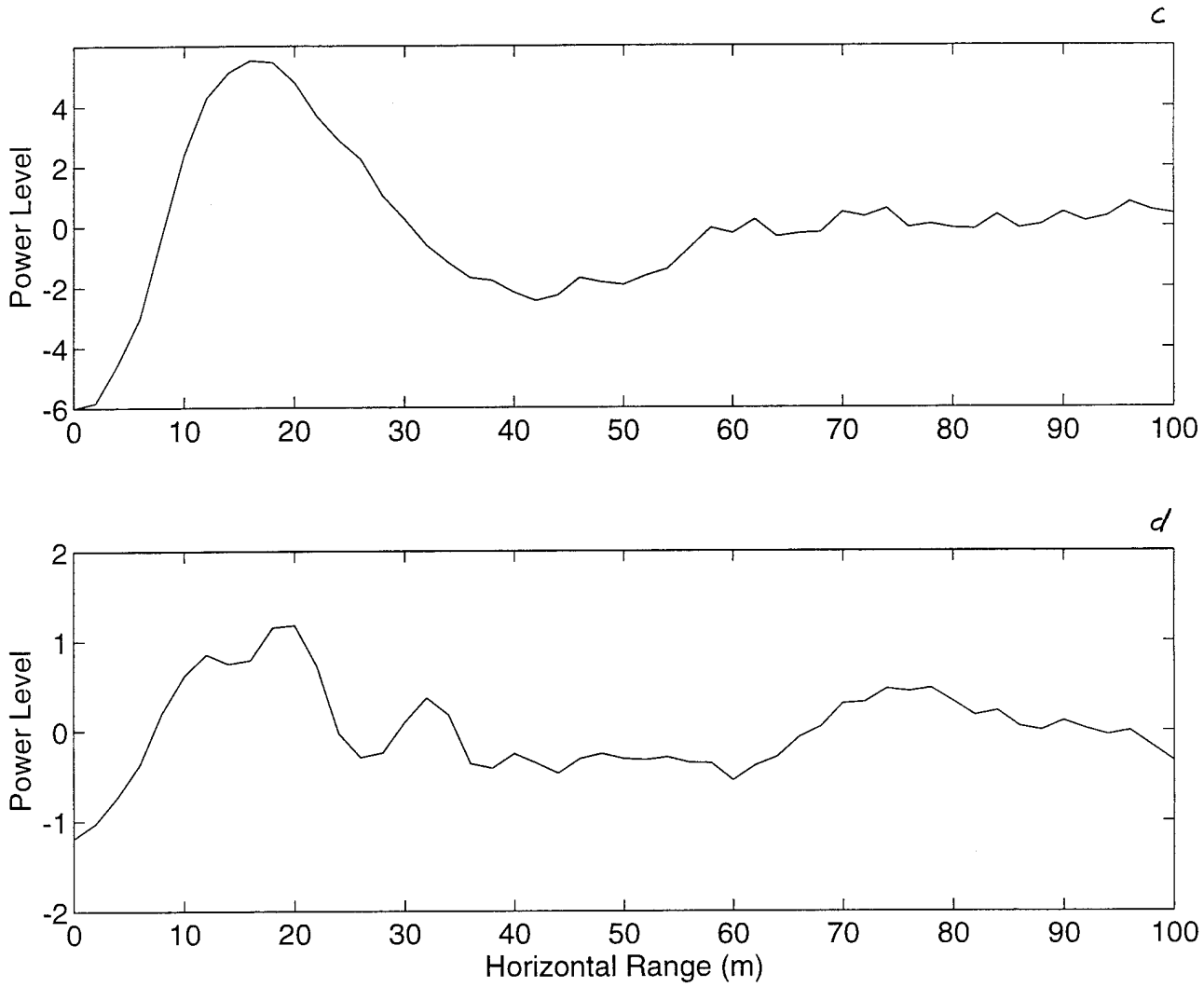
c
Power Level
4
2
0
-2
-4
-6
0
10
20
30
40
50
60
70
80
90
100
d
Power Level
2
1
0
-1
-2
0
10
20
30
40
50
60
70
80
90
100
Horizontal Range (m)

Figure 10c,d.

Focus beamformed output v.s. time
File: tapeE25.10.sio
Start Time: 092:031949

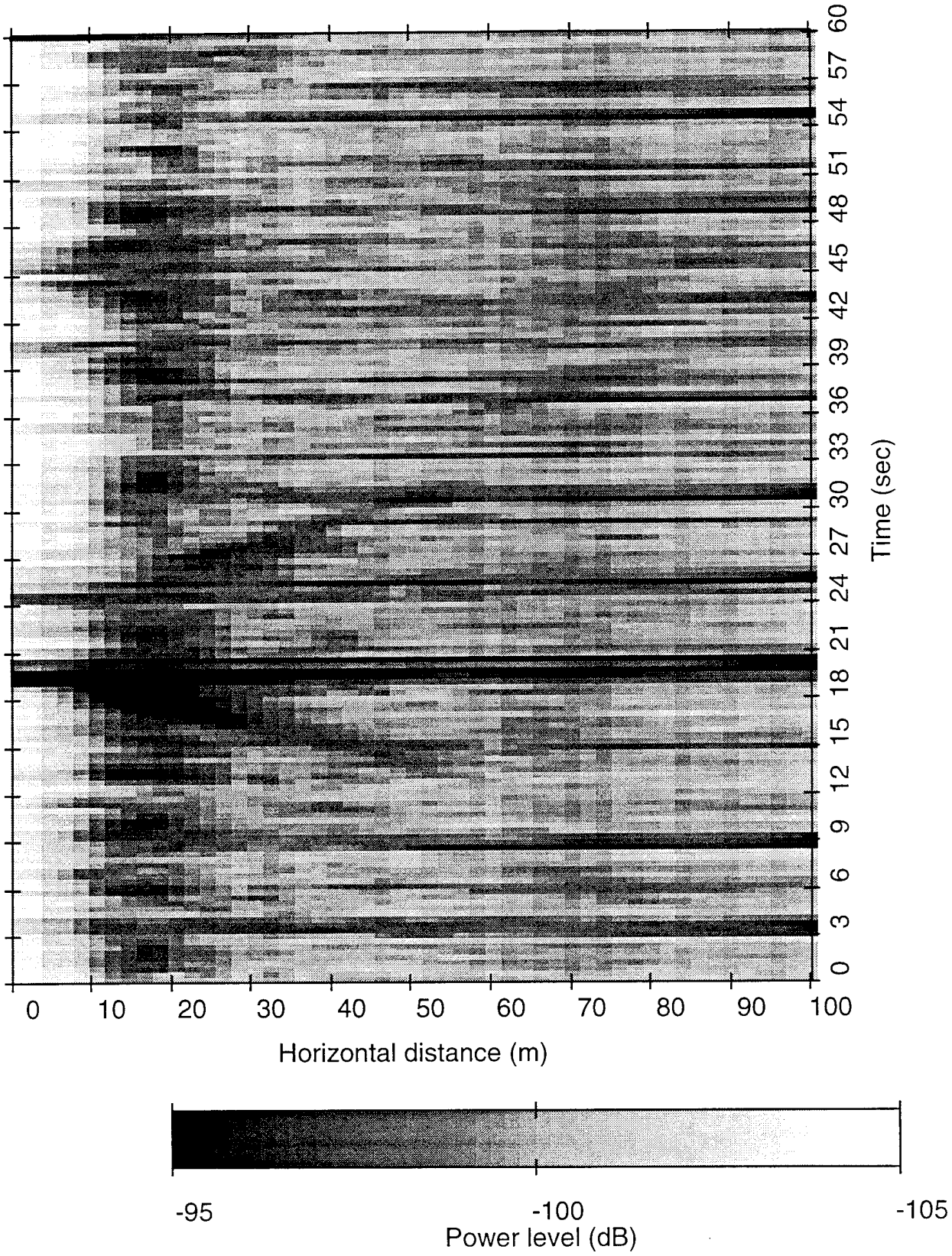

Figure 11a.

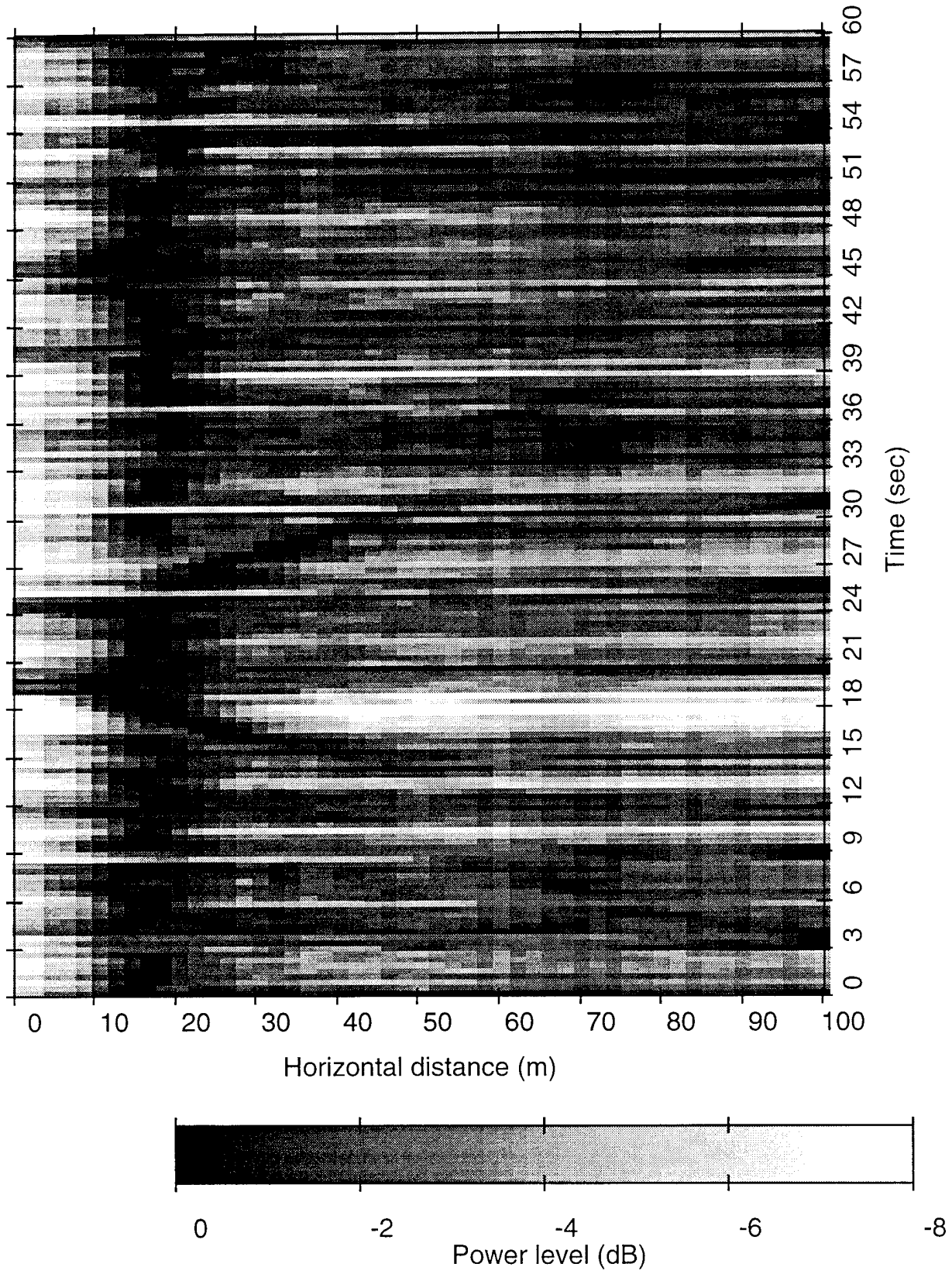
Focus beamformed output v.s. time
File: tapeE25.10.sio, normalized
Start Time: 092:031949
0 3 6 9 12 15 18 21 24 27 30 33 36 39 42 45 48 51 54 57 60
Time (sec)
0 10 20 30 40 50 60 70 80 90 100
Horizontal distance (m)
0 -2 -4 -6 -8
Power level (dB)

Figure 11b.

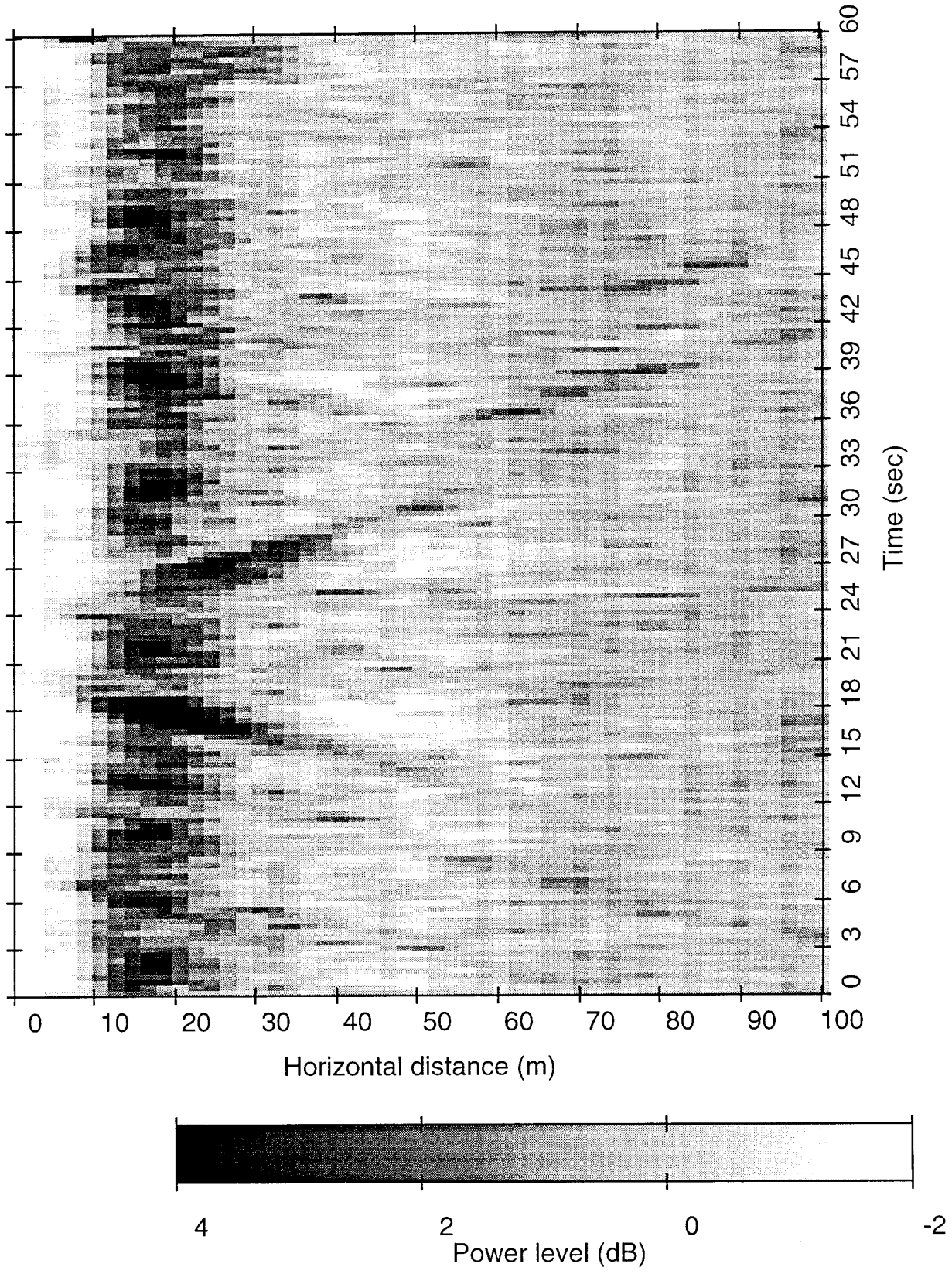
Focus beamformed output v.s. time
File: tapeE25.10.sio, detrended
Start Time: 092:031949
0 3 6 9 12 15 18 21 24 27 30 33 36 39 42 45 48 51 54 57 60
Time (sec)
0 10 20 30 40 50 60 70 80 90 100
Horizontal distance (m)
4 2 0 -2
Power level (dB)

Figure 11c.